Tutora
Dra. Pilar Ramírez de la Piscina
Departament de Química Inorgànica

Grau de Química

Treball Final de Grau

Preparation and characterization of TiO_2-based photocatalysts

Preparació i caracterització de fotocatalitzadors basats en TiO_2

Mireia Broch Gösser

June 2014

Universitat de Barcelona
Campus d'Excel·lència Internacional BKC Barcelona Knowledge Campus

The future belongs to people who see possibilities before they become obvious.

Ted Levitt

En primer lloc vull agrair a tot l'equip d'Investigació de Materials Catalítics del Departament d'Inorgànica de la UB poder realitzar aquest treball amb ells. En particular a Pilar Ramírez de la Piscina, que m'ha guiat amb els seus alts coneixements en el món de la catàlisi. Al realitzar aquest treball he participat en part de la tesi del doctorand Alberto Córdoba Sola, al qual agraeixo moltíssim la ajuda que m'ha donat i, juntament amb els altres membres de l'equip, ha fet que la estància al TFG hagi estat encara més agradable.

En segon lloc agraeixo el suport i ànims que em donen la meva família i els meus amics. Amb ells al costat és sempre més fàcil.

REPORT

CONTENTS

1. SUMMARY

TiO_2 has become one of the most promising photocatalysts for hydrogen production based on the water splitting reaction. The photocatalytic activity of TiO_2 depends on its crystalline phase, crystallinity, crystallite size and surface area. Moreover, there are different ways to increase the photocatalytic activity of TiO_2, such as coupling it with noble metals or adding other semiconductors.

In this research work, 0,5%Pt/TiO_2-x%M (M=In, Ga, Fe, Ru and x=0,19-1,26) photocatalysts have been prepared with two types of TiO_2 with similar textural characteristics but different crystalline phase. The study has particularly focused on the photocatalysts containing indium and gallium. Afterwards, the photocatalysts have been characterized by X-ray diffraction (XRD), Raman Spectroscopy, Brunauer-Emmet-Teller (BET) method, UV–Vis diffuse reflectance spectroscopy (DRS), temperature-programmed reduction-H_2 (TPR) and X-ray photoelectron spectroscopy (XPS).

The characteristics of the catalysts that have been studied are structural, textural and superficial properties, the band gap and the reduction behaviour.

Keywords: TiO_2, photocatalysts, water splitting, band-gap, bimetallic catalysts, incipient wetness impregnation

2. RESUM

TiO_2 s'ha convertit en un dels fotocatalitzadors més prometedors per la producció d'hidrogen basada en la reacció water splitting. L'activitat fotocatalítica de TiO_2 depèn de la seva fase cristal·lina, la cristal·linitat, la mida de cristall i l'àrea superficial. A més a més, existeixen diferents maneres d'incrementar l'activitat fotocatalítica de TiO_2, tal com acoblar-la amb metalls nobles o afegir altres semiconductors.

En aquest treball s'han preparat fotocatalitzadors del tipus 0,5%Pt/TiO_2-x%M (M=In, Ga, Fe, Ru i x=0,19-1,26) amb dos tipus de TiO_2 amb característiques texturals semblants però diferent fase cristal·lina. L'estudi s'ha centrat particularment en els fotocatalitzadors amb indi i gal·li. Posteriorment s'han caracteritzat per difracció de raig-X (XRD), espectroscòpia Raman, mètode de Brunauer-Emmet-Teller (BET), espectroscòpia de reflectància difusa UV–Vis (DRS), reducció a temperatura programada-H_2 (TPR) i espectroscòpia fotoelectrònica de raig-X (XPS).

Les característiques dels catalitzadors que s'han estudiat són propietats estructurals, texturals i superficials, el band gap i el comportament de reducció.

Paraules clau: TiO_2, fotocatalitzadors, water splitting, band-gap, catalitzadors bimetàl·lics, impregnació d'humitat incipient

3. INTRODUCTION

3.1. WATER SPLITTING

Light-driven water splitting to produce hydrogen is a promising way to solve the increasing global concerns on fossil energy and climate problems [1]. Since the discovery of Honda and Fujishima that H_2O could be decomposed into H_2 and O_2 with a photoelectrochemical cell consisting of Pt and TiO_2 electrodes under a small electric bias, photocatalytic generation of H_2 over TiO_2 based photocatalyst has been extensively studied [2].

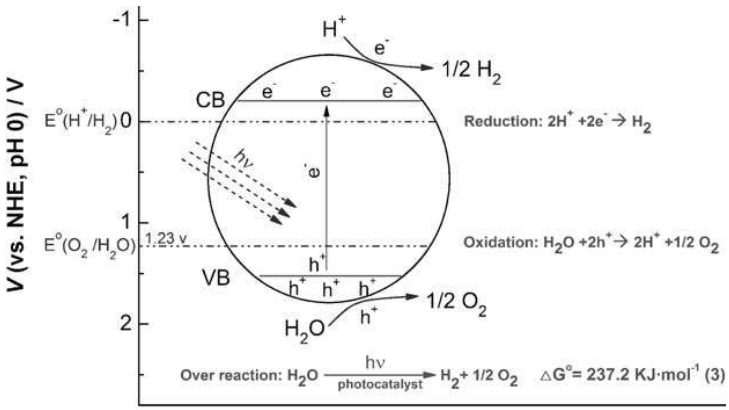

Figure 1.a. Watter splitting reaction

In Figure 1.a [2] the water-splitting process on a semiconductor photocatalyst is represented. Semiconductors possess an empty region in which no energy levels are available, called band gap (Eg), which is located between the highest occupied energy band, called valence band (VB), and the lowest empty band, called conduction band (CB). When the energy of an irradiated photon is larger than Eg, electrons (e^-) can be excited from the VB into the CB, leaving holes (h^+) in the VB. Whether or not the water-splitting reaction then occurs is determined by the electronic band structure of the photocatalyst. For water reduction, the CB potential must be more negative than the H^+ reduction potential of H^+/H_2 [0.0 V vs. the normal hydrogen electrode (NHE)]. To facilitate the oxidation of water by h^+, the VB edge must be more positive than the oxidation potential of O_2/H_2O [1.23 V vs. NHE]. Considering this, the theoretical minimal band gap for water splitting is 1.23 eV, which corresponds to a wavelength

of about 1010 nm. Although theoretically about 70% of solar photons can be used for water splitting, in practice, considering energy losses, this amount decreases considerably [2].

After the generation of e^- and h^+, the steps that follow are their separation, migration from the bulk to the surface, and the actual water-splitting reaction on the surface. The charge transport efficiency is strongly affected by the crystal structure, crystallinity, and crystallite size of the sample. High crystallinity and small crystallite size can decrease the probability of recombination of e^- and h^+ [2].

3.2. TiO_2

TiO_2 can crystallize in three different structures: anatase, rutile, and brookite. The first and second phases have most often been used as photocatalysts for hydrogen production [3]. For bulk TiO_2, the band gaps of anatase and rutile are 3.2 and 3.0 eV [2]. Although rutile should theoretically show more photoactivity for hydrogen generation, it has been proved in many investigations that it is higher using the anatase phase. This is due to their different electronic band structures: the CB potential of rutile coincides almost with the NHE potential, whereas that of anatase is shifted cathodically by almost 0.2 V. Therefore, the driving force for water reduction is very small for rutile while the reduction takes place more easily in the anatase form.

The photocatalytic activity of TiO_2 for H_2 evolution can be enormously improved by good selection of the structure, the crystallinity, the crystallite size, and the surface area of TiO_2 and doping it with noble metals ar adding other semiconductors.

3.2.1. TiO_2 modifications

There are some drawbacks that make the photocatalytic activity of TiO_2 very low: first of all, the required large overpotential for the evolution of H_2 and O_2. Second, the fast recombination of photoinduced e^- and h^+ before migrating to the surface to split water (about 90% of photogenerated carriers recombine after excitation) [4]. Third, the inability to make use of visible light as the band gap of TiO_2 is about 3.2 eV and only ca. 4–5% of the solar light can be used for H_2 production, while the other ca. 40% of visible light can not be utilized [5].

Therefore, there are many possible modifications of TiO_2 such as coupling with noble metals, doping TiO_2 with other ions, coupling with other semiconductors and adding sacrificial reagents

to the reaction solution [2]. Some of the possible strategies to increase the photoactivity of TiO_2 are described in more detail below.

Decreasing the overpotential for H_2 evolution can be achieved by loading TiO_2 with co-catalysts of noble metals, such as Pt, Pd, Au, Rh, and Ag. These metals have a low overpotential for hydrogen, which can make it easier to generate H_2. The metals can thus serve as active sites for H_2 production on the TiO_2 surface (as shown in Figure 1.b [2] where Pt and RuO_2 have been added).The lower the overpotential of the metal, the higher the activity it shows. Among the cited metals, Pt is the most widely used because it has the lowest overpotential and shows the highest activity for H_2 generation [6].

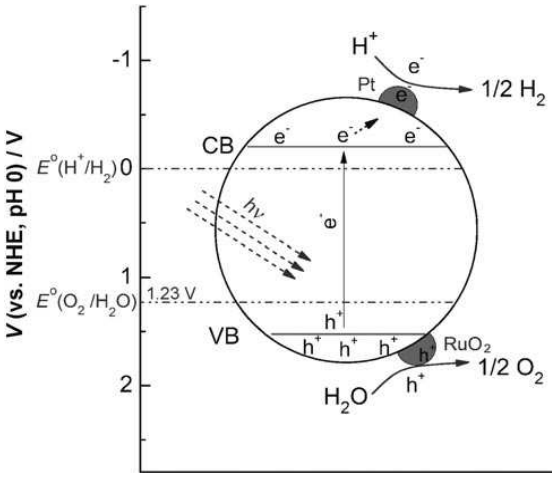

Figure 1.b. Water splitting process of TiO_2 loaded with Pt and RuO_2

The process of recombination of the carriers (e^- and h^+) can occur in two different processes: in the charge transfer from the bulk to an active site or during interfacial charge transfer from an active site to an H_2O molecule. The transportation rate can be improved by increasing the crystallinity of TiO_2 or by loading TiO_2 with noble metals, such as Pt. This noble metal helps to inhibit the recombination of the carriers by acting as an electron trap [7]. The survival time of the charges on the surface can be prolonged by coupling TiO_2 with other semiconductors or by adding sacrificial reagents to the reaction solution [2].

Semiconductors that possess different redox energy levels, on account of their corresponding CB and VB, can help to achieve a more efficient charge separation. When TiO_2 and the semiconductor are activated by light, photoinduced e^- would be injected from the semiconductor with a more negative CB level to the positive one, while h^+ would be transferred from the semiconductor with a more positive VB level to the negative on, as can be seen in a general process in Figure 1.c [8]. Therefore, a wide separation of photoinduced charges is achieved, which consequently increases their lifetime as well as the efficiency of the interfacial charge transfer to water. Some semiconductors that have been satisfactory used are In_2O_3, Fe_2O_3, CdS, ZnO, SiC, Cu_2O, CuO, SnO_2, WO_3, V_2O_5, and others.

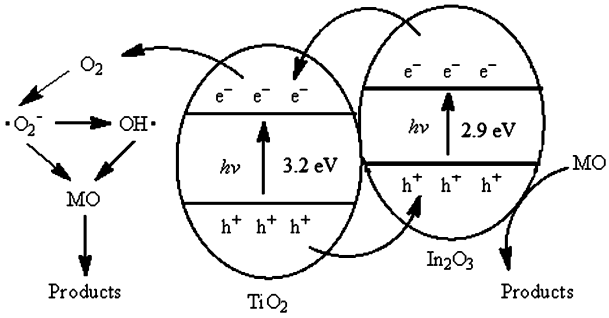

Figure 1.c. Charge separation in In_2O_3/TiO_2 semiconductor combination system

Another way to enhance the photocatalytic activity of TiO_2 is adding a sacrificial reagent to the reaction solution. These can be electron donors or acceptors, which are more easily oxidized or reduced. Sacrificial agents that act as hole scavengers are, for example, organic compounds such as methanol, ethanol, lactic acid, formaldehyde, CN^- and EDTA, as well as some biomass-derived carbohydrates. The chemical reaction that occurs when a sacrificial agent such as methanol is present in the reaction solution is the oxidation of CH_3OH by h^+, and the following reduction of H^+ by e^-.

Considering the possible improvements that can be done on TiO_2, the aim of this work is to prepare and characterize TiO_2-based photocatalysts adding 0.5 wt% of Pt and different content of M (M=Ga, In, Fe, Ru)

Once the modifications of TiO_2 have been analyzed, the photocatalysts will be tested in reaction within the framework of the PhD of Alberto Córdoba Sola.

3.3. PHOTOCATALYST CHARACTERIZATION TECHNIQUES

In order to study the modifications done on TiO_2 , there are many possible characterization techniques that can be carried out on the samples. The relevant information that can be obtained from each technique will be explained in the next paragraphs:

3.3.1. Powder X-ray diffraction

XRD is a technique used to identify bulk phases and to estimate crystallite size. The crystalline atoms cause a beam of incident X-rays to diffract into many specific directions. The angles and intensities of the diffracted beams are measured [9]. From this information diffraction patterns can be obtained, and there is one for each material that presents crystallinity. These diffraction patterns can be found in different XRD databases.

In this work, XRD has been used to identify the crystalline phases in the catalysts: anatase, rutile and brookite for TiO_2, and other possible phases of the added compounds; calculate the crystallite size and determine the anatase/rutile ratio.

3.3.2. BET

The Brunauer–Emmett–Teller (BET) theory serves to explain the physical adsorption of gas molecules on a solid surface, which is used to obtain the surface area, the pore size distribution and the pore volume of the material. This theory is based on the Langmuir equation which is applied on monolayer molecular adsorption, and the BET extends to multilayer adsorption with the following hypotheses: (a) gas molecules physically adsorb on a solid in layers infinitely; (b) there is no interaction between each adsorption layer; and (c) the Langmuir theory can be applied to each layer.

The specific surface area of a material is determined by physical adsorption (Van der Waals attraction) of a gas, such as N_2 at a temperature in which N_2 is liquid, on the surface of the solid, and by calculating the amount of adsorbate gas corresponding to a monomolecular layer

on the surface. The amount of gas adsorbed can be measured by volumetric or continuous flow procedure [9], [10], [11].

Adsorption isotherms are obtained by measuring the amount of gas adsorbed across a wide range of relative pressures at a constant temperature (usually 77K for N_2). Desorption isotherms are achieved by measuring gas removed as pressure is reduced.

The BET equation (eq. 1) to describe specific surface area is [12]:

$$\frac{p}{n^a \cdot (p^o - p)} = \frac{1}{n^a_m \cdot C} + \frac{(C-1) \cdot p}{n^a_m \cdot C \cdot p^0}$$

Equation 1. BET

Where: n^a is the amount adsorbed at the relative pressure p/p^o and n^a_m is the monolayer capacity.

3.3.3.Ultraviolet-visible diffuse reflectance spectroscopy

This technique can refer to absorption spectroscopy or reflectance spectroscopy in the ultraviolet-visible spectral region. From the UV-vis diffuse reflectance spectra it is possible to calculate the band gap, this is, the energy difference between the top of the valence gap and the bottom of the conduction band; e^- are able to jump from one band to another. The value of the band gap is very significant in semiconductor materials, specifically in this work it is aimed to decrease the band gap for the reasons explained in the introduction. The UV-vis reflectance has been done on the bulk supports and on the modified samples, in order to study the band gap modification.

3.3.4. Raman spectroscopy

Raman is a spectroscopic technique based on inelastic scattering of monochromatic light, usually from a laser source. Inelastic scattering means that the frequency of photons in monochromatic light changes upon interaction with a sample. Photons of the laser light are absorbed by the sample and then reemitted. Frequency of the reemitted photons is shifted up or down in comparison with original monochromatic frequency, which is called the Raman

effect. This shift provides information about vibrational, rotational and other low frequency transitions in molecules [13].

Raman was carried out in this work as a complementary technique to XRD to identify the crystalline phases of the catalysts and to study the possible presence of crystalline phases in the formation of new species.

3.3.5. Temperature-programmed reduction-H_2

Technique that gives the H_2 consumption required to reduce the reducible species in the given conditions present in the sample and reveals the temperature at which the reduction of each species occurs.

A TPR analysis consists in flowing a gas (typically hydrogen in an inert carrier gas such as nitrogen or argon) through the sample usually at RT. While the gas is flowing, the temperature of the sample is increased with time and the consumption of hydrogen by adsorption/reaction is monitored. Changes in the concentration of the gas mixture downstream from the reactor are determined. This information yields to the total consumed volume of H_2 [9], [14].

In this work TPR has been executed in order to determine the reduction temperature of platinum and to study the possible reduction of other species that are present in the photocatalysts.

3.3.6. X-ray photoelectron spectroscopy

XPS is one of the most widely used surface analysis technique. It consists in the irradiation of the sample with mono-energetic X-rays causing photoelectrons to be emitted from the sample surface; it is only used for surface analysis due to the short range of the photoelectrons that are excited from the solid. The binding energy is obtained from the equation: $E_k = hv - E_b - \phi$, based on the photoelectric effect: an atom absorbs a photon of energy hv; a core or valence electron with binding energy E_b is ejected with kinetic energy, and ϕ is the work function of the spectrometer [9], [15]. From the BE and intensity of a photoelectron peak, the elemental identity, chemical state, and content of an element are determined. The shape of each peak and the BE can be slightly altered by the chemical state of the emitting atom.

XPS has been performed in this work in order to study the surface composition. The atomic ratios have been obtained from the XPS spectra and the sensitivity factors which are characteristic of each atom and each level.

3.3.7. Inductively coupled plasma spectrometry

ICP analytical techniques can quantitatively measure the elemental content of a material from the ppt to the wt% range. Solid samples are dissolved or digested in a liquid, usually an acidic aqueous solution. The sample solution is sprayed into the core of an inductively coupled argon plasma, which reaches temperatures of aprox. 8000ºC. At such temperatures, all analyte species are atomized, ionized and thermally excited, and they can then be detected and quantified with an emission spectrometer (OES) [16].

ICP has been used in order to determine the exact wt% of the deposited metals.

4. OBJECTIVES

Taking into account the possible modifications that can be done on TiO_2 in order to increase its photocatalytic activity and knowing the techniques that can be useful to characterize the catalysts, the main objectives of this work are:

-To prepare 0.5wt%Pt/TiO_2-M photocatalysts (M=In, Ga, Fe, Ru), using two TiO_2 supports with similar textural characteristics but different crystaline phase composition. The M content is in the range 0.4-2.4 atoms per nm^2 of support.

-To study the structural, textural and superficial characteristics, the band gap modification and the reduction behaviour of the photocatalysts using the characterization techniques XRD, Raman spectroscopy, BET, TPR, DRS and XPS.

5. EXPERIMENTAL

5.1. CHEMICALS

-TiO_2 Degussa P25

-TiO_2 Sigma Aldrich

-$H_2PtCl_6 \cdot 6H_2O$

-$In(NO_3)_3 \cdot xH_2O$

-$Ga(NO_3)_3 \cdot xH_2O$

-$Fe(NO_3)_3 \cdot 9H_2O$

-$RuCl_3$

-Water HPLC grade

5.2. PREPARATION OF PHOTOCATALYSTS

In this work, 9 different photocatalysts have been prepared (weight: 3 g) using commercial TiO_2 as a support in two different forms: Degussa P25 (anatase:rutile ratio 4:1) and Sigma Aldrich (anatase). All the samples contain around 0.5 wt% of Pt and different weight percentage of indium, gallium, iron or ruthenium.

They have been named following the next pattern: Pt/A-xM or Pt/AR-xM where A is Sigma Aldrich TiO_2 and AR is Degussa P25 TiO_2; M=In, Ga, Fe or Ru and x is the wt% of M in the range 0.19-1.26 %.

The photocatalysts have been prepared by the incipient wetness impregnation, which consists in filling all the pores of the support with the metal precursor aqueous solution.

The first step is the impregnation of the support with the solution that contains the precursor of the co-dopant M (M=In, Ga, Fe, Ru) equivalent to the desired wt%. After that, the photocatalyst is dried in the oven at 80ºC for 2h, and finally it is calcined at 400ºC for 30 min, with a heating rate of 100ºC/h. The second step is the impregnation with the solution of the precursor of platinum equivalent to 0.5 wt%. Afterwards, it is dried at 80ºC for 1 h, and finally it is calcined at 400ºC for 4 h with a heating rate of 5ºC/min.

5.3. CHARACTERIZATION EQUIPMENTS AND CONDITIONS

5.3.1 ICP

The content of Pt, In, Ga, Fe, Ru and TiO_2 was determined by inductively-coupled plasma atomic emission spectrometry using a Perkin Elmer Optima 3200RL equipment.

5.3.2 X-ray diffraction

X-ray diffraction analysis of the samples was performed on a Xpert PRO-diffractometer equipped with a CuKα radiation source (λ=1.5406 Å) and a graphite monochromator. The XRD patterns were collected between 2θ=20º-100º, with a step width of 0.05º counting 3 s at each step.

The average crystallite size was estimated using the Scherrer equation, $D = k \cdot \lambda / \beta_{2\theta} \cdot \cos \theta_{max}$, where k is a constant which depends on the morphology of the crystalline phases presented (k=1), λ is the X-ray wavelength, $\beta_{2\theta}$ is the width of the anatase (1 0 1) and rutile (1 1 0) diffraction peaks at half-height, and $\cos \theta_{max}$ is the Bragg angle at the peak maximum position [17].

The rutile/anatase ratio can be also calculated from the XRD data according to the formula [18]:

$$W_R = \frac{A_R}{0.884A_A + A_R}$$

Equation 2. Percentage of rutile phase

Where W_R is the percentage of rutile, and A_A and A_R are, respectively, the integrated areas of the (1 0 1) peak of anatase and the (1 1 0) peak of rutile.

5.3.3 Nitrogen adsorption/desorption

According to the Brunauer–Emmett–Teller (BET) and Barrett–Joyner–Halenda (BJH) approaches, specific surface areas, pore volumes and pore size distribution of the powder samples were determined by N_2 adsorption-desorption isotherms at 77 K using a Micromeritics TriStar II 3000 apparatus. The degasification of the sample was carried out at 250ºC for 5h under N_2 flow.

5.3.4 UV–vis diffuse reflectance

The UV–Vis spectra of the samples were obtained with a PerkinElmer Lambda 950 UV/Vis Spectrometer with a 3 nm slit width, and a speed of 654.92 nm·min^{-1}. $BaSO_4$ was used as reference.

The reflectance spectra were analyzed using the Kubelka-Munk formalism to convert the reflectance into the equivalent absorption coefficient, where R∞ is the reflectance of an infinitely thick sample with respect to a reference at each wavelength.

$$F(R_\infty)=\frac{(1-R_\infty)^2}{2R_\infty}$$

Equation 3. Kubelka-Munk formalism

Band gap values of all photocatalysts have been calculated by linearization of the slope to the X axis (wavelength, nm) with the Y axis ((F(R∞)·hv)^n). This process for obtaining Band Gap is called Tauc Plot, where n=1/2 denotes a directly allowed transition [19].

5.3.5 Raman spectroscopy

The Raman spectra of the samples were measured using a Jobin-YvonLabRam HR 800 in micro-Raman mode equipped with a CCD detector coupled with an Olympus BXFM optical microscope. The samples were excited with the 532 nm solid state laser. The spectrum acquisition consisted in 3 accumulations of 5 s for each sample. The samples were studied at 50x magnification. Laser power was limited at 1.5 mW.

5.3.6 TPR

Temperature programmed H_2-reduction was performed using a Micromeritcs Autochem II 2920 system. The reduction profiles were obtained by passing a flow with 10% H_2/Ar at a rate of 50 cm^3·min^{-1} (STP) through the sample (around 50 mg) placed in a U-shaped quartz reactor. The temperature was increased from 253 K to 973 K at a heating rate of 10 º·min^{-1}, and the amount of hydrogen consumed was determined on a thermal conductivity detector (TCD) as a function of temperature.

6. RESULTS AND DISCUSSION

Table 1 lists the characteristics of the supports A and AR, and the prepared photocatalysts. The content of Pt and the co-doped M has been obtained by ICP. As can be observed, the wt% of Pt that has been obtained in all the samples is near the desired value.

Table 1. Characteristics of supports and photocatalysts

Name	wt% of Pt	wt% of M	M atoms /nm^2 TiO_2	Crystallite size (nm) Anatase/Rutile	%wt of Rutile phase	Surface area (m^2/g)	Pore volume (cm^3/g)	Band gap (eV)
A (Aldrich)	-	-	-	26/-	-	45.0	0.27	3.20
AR (P25)	-	-	-	26/49	14.4%	51.3	0.22	3.04
Pt/A-1.14In	0.49	1.14	1.3	26/-	-	45.9	0.24	3.15
Pt/A-1.43In	0.44	1.43	1.7	26/-	-	45.7	0.23	3.13
Pt/AR-1.90In	0.42	1.9	1.8	27/48	13.5%	45.7	0.25	2.95
Pt/A-0.19Ga	0.51	0.19	0.4	26/-	-	45.7	0.24	3.14
Pt/A-0.61Ga	0.47	0.61	1.2	26/-	-	45.5	0.24	3.15
Pt/A-1.26Ga	0.45	1.26	2.4	26/-	-	44.5	0.24	3.15
Pt/AR-0.77Ga	0.47	0.77	1.2	27/47	14.2%	47.0	0.28	2.93
Pt/A-0.75Fe	0.48	0.75	1.8	25/-	-	44.9	0.24	2.96
Pt/A-0.29Ru	0.46	0.29	0.4	26/-	-	46.2	0.26	3.01

In Figure 2.a, 2.b and 2.c the XRD patterns of the supports A and AR, and the obtained photocatalysts are shown.

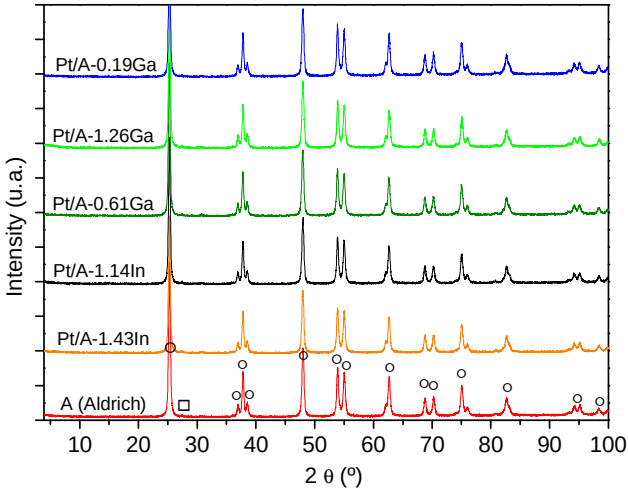

Figure 2.a. XRD pattern of A, Pt/A-Ga and Pt/A-In samples

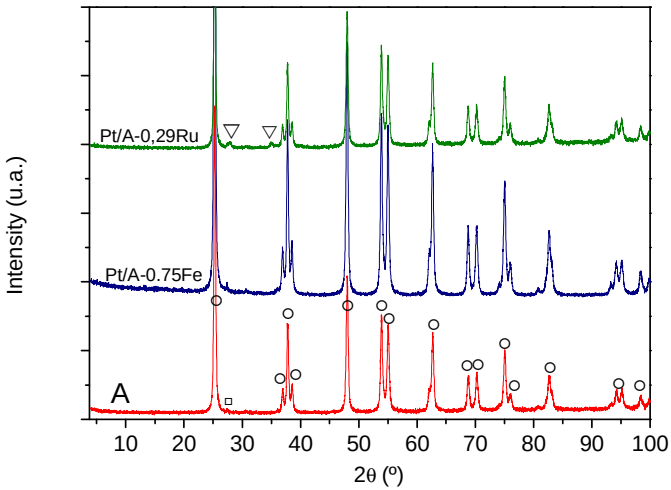

Figure 2.b. XRD pattern of A, Pt/A-Fe and Pt/A-Ru samples

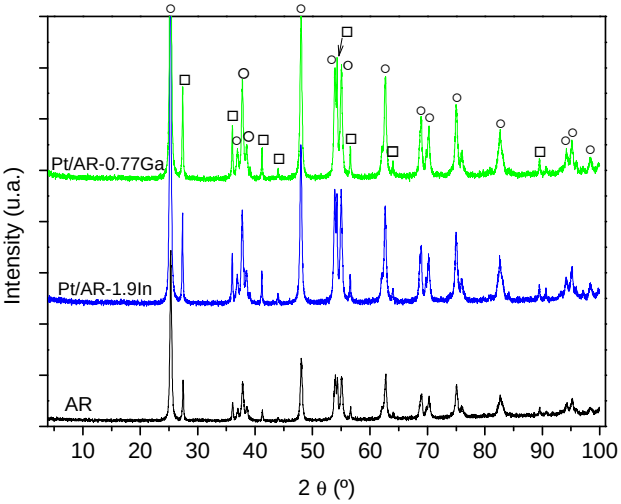

Figure 2.c. XRD pattern of AR, Pt/AR-In and Pt/AR-Ga samples

In the XRD patterns of A and all the Pt/A-M samples (Figure 2.a and 2.b), the characteristic peaks of the anatase phase can be found. The most intense peaks are marked with a circle symbol (JCPDS 00-021-1272). Moreover, a peak of the rutile phase with a very low intensity at 27.5º can be seen; it is marked with a square symbol. (JCPDS 01-077-0446). As can be observed, the intensity of the rutile peak is not altered by the metal deposition. Moreover, in the Pt/A-0.29Ru XRD pattern, there are also two minor peaks present that correspond to RuO_2, at 28º and 35º (JCPDS 00-021-1172).

In the XRD spectra of AR and the Pt/AR-M samples, the most intense peaks of both phases anatase and rutile are present, marked with “circle” and “square”. The weight fraction of rutile of the support and the catalysts has been calculated [18], and it has not been altered after the metal deposition. No other peaks corresponding to possible compounds of the deposited metals have been found in the XRD patterns of the catalysts.

The crystallite size of the anatase and rutile phase of the samples has been calculated on the basis of the full widths at half-maximum of the anatase peak (101) and the rutile peak (110) [17]. The values are shown in Table 1. In the A and AR based samples, the crystallite size of

the anatase phase has barely changed respect the one of the support (26 nm). When it comes to the crystallite size of the rutile phase, which is quite larger than the anatase phase crystallite size (~47 nm) [20], this has not been altered by adding Pt and In or Ga. It can be concluded that the metal deposition in this wt% range does not affect the crystallite size of the support, nor the anatase/rutile ratio.

Raman spectroscopy has been performed on the photocatalysts as a complementary technique to XRD in order to identify the crystalline phases. Figure 3.a, 3.b (see Appendix) and 3.c show the Raman spectra of A, AR and the prepared photocatalysts.

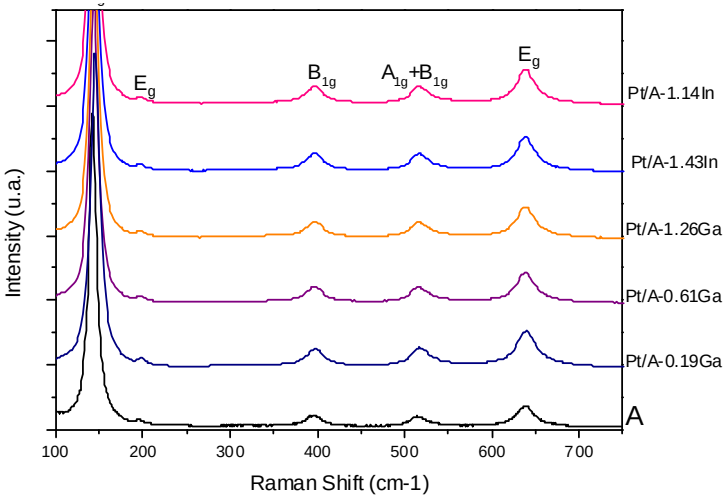

Figure 3.a. Raman spectra of A, Pt/A-In and Pt/A-Ga samples

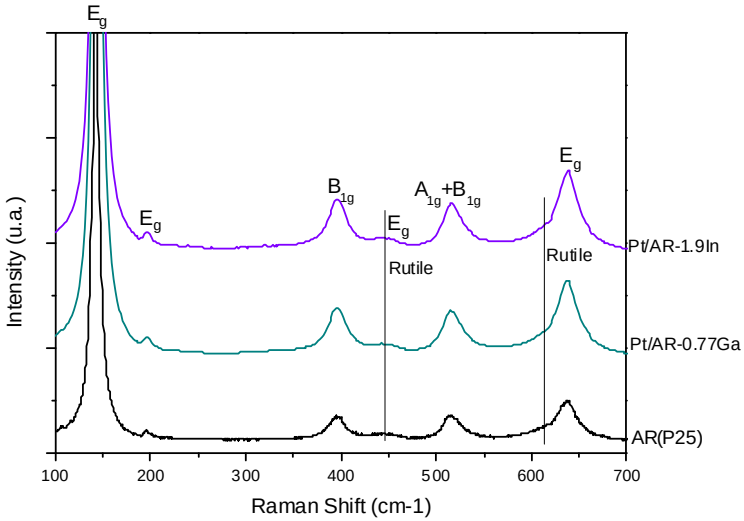

Figure 3.c. Raman spectra of AR, Pt/AR-In and Pt/AR-Ga samples

In the Raman spectra of A and the Pt/A-M samples, the characteristic bands of the anatase phase are clearly appreciable: 142 (Eg), 195 (Eg), 395 (B1g), 515 and 637 (Eg) [21]. No rutile phase bands are present.

In Figure 4.3 the Raman spectra of AR and the samples Pt/AR-1.9In and Pt/AR-0.77Ga can be observed. Both anatase and rutile phase bands are appreciable. The bands corresponding to the rutile phase appear at ~ 446 cm^{-1} and ~610cm^{-1} [22].

From the Raman spectra of the samples, it can be concluded that the deposition of metals and the posterior calcination have not changed the anatase/rutile ratio. Otherwise, the formation of any other possible compound, as could be an oxide of these metals, has not been observed. These facts confirm what has been seen in XRD.

Figure 4.a, **4.b** and **4.c** (see Appendix) show the N_2 adsorption/desorption isotherms of the supports A and AR, and the prepared photocatalysts.

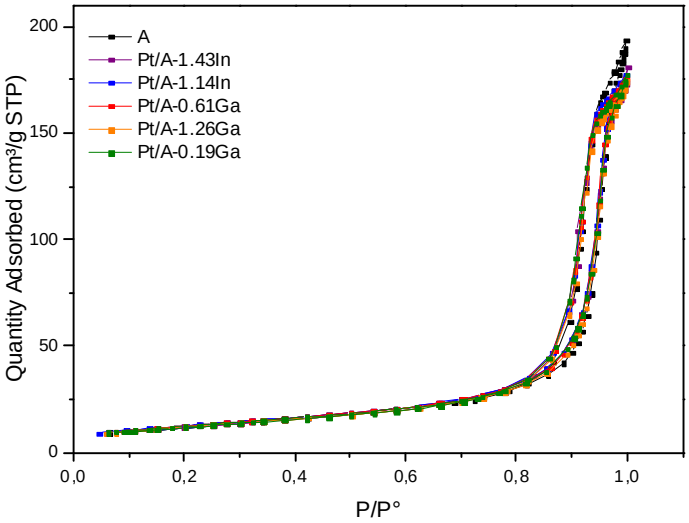

Figure 4.a. N_2 adsorption/desorption isotherm of A, Pt/A-In and Pt/A-Ga samples

It can be considered that the isotherm of the supports and the prepared photocatalysts is Type IV, according to the IUPAC [12]. The distinctive feature of this type of isotherm is the presence of a hysteresis loop. This type of isotherm is characteristic of mesoporous solids. The hysteresis loop is associated with capillary condensation taking place in mesopores, and the limiting uptake over a range of high p/pº. The initial part of the isotherm is attributed to monolayer-multilayer adsorption.

The hysteresis loop of both supports and the Pt/A-M and Pt/AR-M photocatalysts is type H1 (IUPAC). Type H1 is often given for adsorbents with a narrow distribution of uniform pores [23]. However, the shape of the hysteresis loop of AR is slightly different; this could be related to the pore size distribution, which is wider for AR, as seen in Figure 5.c.

Figure 5.a, 5.b (see Appendix) and 5.c show the pore size distribution of A, AR and the prepared photocatalysts; these have been represented from the BJH Desorption dV/dlog(D) Pore Volume data.

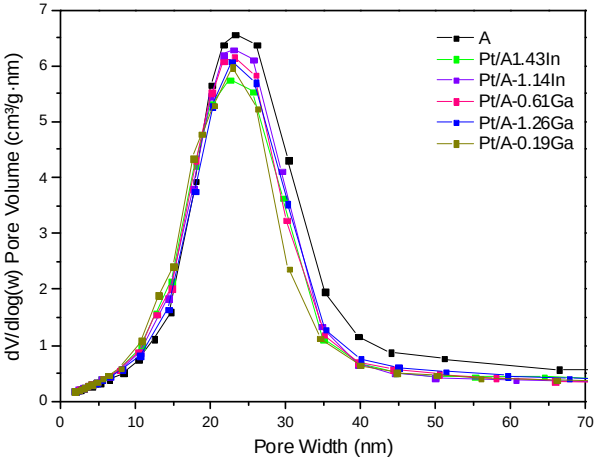

Figure 5.a. Pore size distribution of A, Pt/A-In and Pt/A-Ga samples

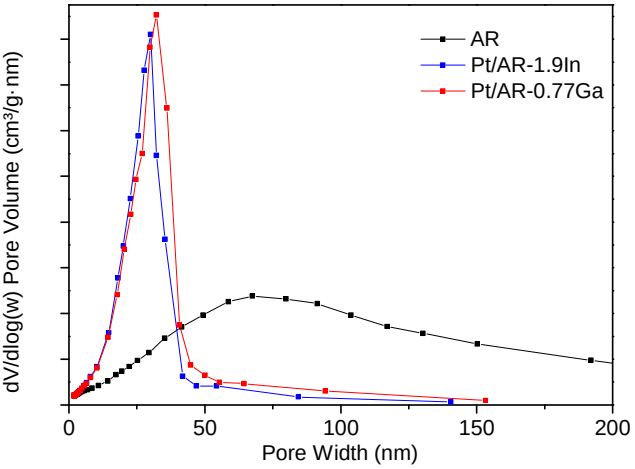

Figure 5.c. Pore size distribution of AR, Pt/AR-In and Pt/AR-Ga samples

The pore size distribution of A has not been affected after the metal deposition and concentrates around 20-30 nm.

Nevertheless, the pore size distribution of AR is very wide (20-150 nm), and after the metal deposition the distribution becomes very narrow around 30 nm.

Table 1 lists the surface area and the pore volume of the doped and undoped A and AR.

The surface area of the Pt/A-M photocatalysts has barely changed with respect to the one of the support. In the case of the Pt/AR-M catalysts, both Pt/AR-1.9In and Pt/AR-0.77Ga have experienced a slight decrease of the surface area, but which is still very low. When it comes to the pore volume of the Pt/A-M and Pt/AR-M photocatalysts, the obtained values are very similar to the pore volumes of the supports.

It can be concluded that the metal deposition on the supports does not affect the surface area nor the pore volume. Nevertheless, in the Pt/AR-M catalysts, the pore size distribution has changed from a wide to a narrow distribution around 30 nm, which corresponds to the pore size distribution of the Pt/A-M catalysts.

Band gaps of all photocatalysts have been obtained through the Tauc-Plot method, as shown in Figure 6.a, **6.b** and **6.c** (see Appendix).

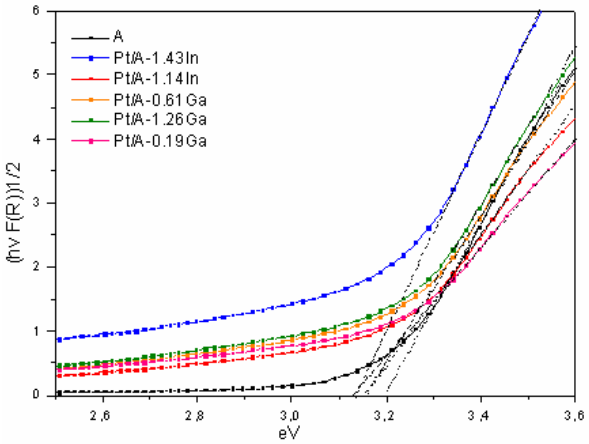

Figure 6.a. Tauc-Plot representation of A, Pt/A-In and Pt/A-Ga samples

The band gap values of all the photocatalysts have decreased respect the Eg of the supports after the metal deposition. The Eg decrease has been significantly higher in the Pt/A-0.29Ru and Pt/A-0.75Fe catalysts. The samples with the smallest band-gap value are the Pt/AR-M catalysts.

Figure 7.a, 7.b and 7.c show the TPR profile of the prepared photocatalysts. Table 2 lists the maximum temperature of the reduction peaks and the experimental H_2 consumption for each sample.

The required amount of H_2 to reduce the content of Pt in each photocatalyst, considering that it is present in the maximum oxidation state, Pt^{4+}, according to the reaction: $PtO_2 + 2H_2 \rightarrow Pt + 2H_2O$ is aprox. 0.003 mmol. As can be noticed in Table 2, the experimental H_2 consumption has been higher in all photocatalysts. This is related to the partial reduction of the oxide of the co-doped metal.

In the TPR profiles of the Pt/A-In samples, a wide tail of H_2 consumption is observed in the temperature range 100-150 ºC, which possibly indicates the In^{n+} reduction. The reduction peaks that appear at the lowest temperatures are the ones of the Pt/AR-M catalysts. This could be due to a higher affinity of Pt with AR than with A, because of the rutile presence.

Moreover, it stands out that the peaks that correspond to the reduction of the co-doped metals appear at lower temperatures than if they were alone. This can be related to the Pt spillover mechanism of H_2, which consists in the adsorption of molecular hydrogen followed by its dissociation and migration of the atomic hydrogen from the metal to the support bulk [24], which makes the co-doped metals more easily reducible. The TPR profile of the Pt/A-0.29Ru sample shows two reduction peaks, which remarks with more clarity the reduction of both Pt and the co-doped metal.

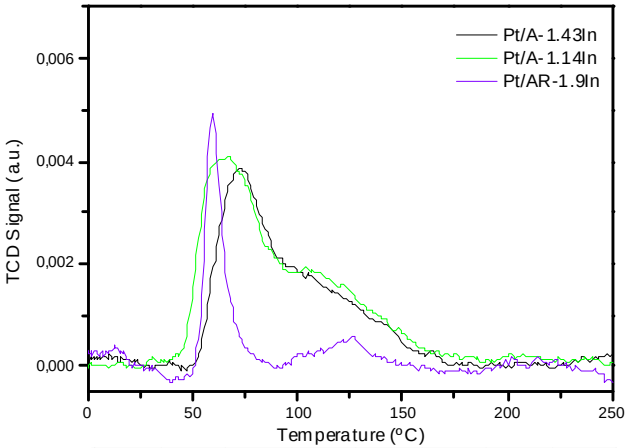

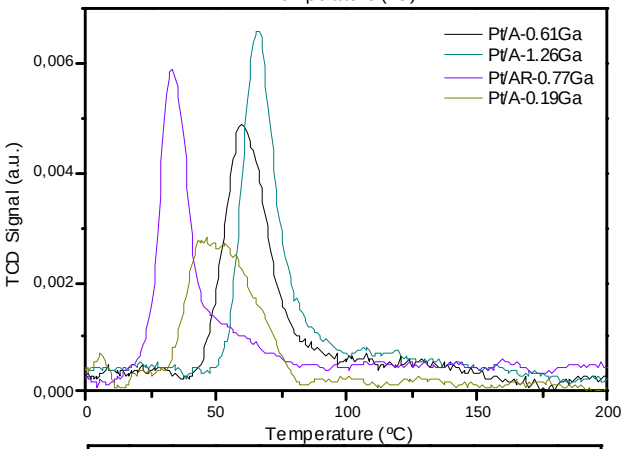

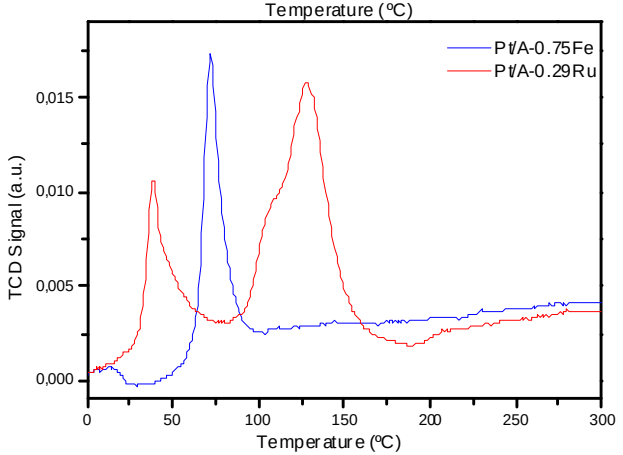

Figure 7.a,7.b and 7.c. TPR profile of the photocatalysts

Table 2. Maximum reduction temperature and H_2 cosumption of the photocatalysts

Sample	Pt/A-1.14In	Pt/A-1.43In	Pt/AR-1.9In	Pt/A-0.19Ga	Pt/A-0.61Ga	Pt/A-1.26Ga	Pt/AR-0.77Ga	Pt/A-0.75Fe	Pt/A-0.29Ru
Tmax. (ºC)	63.3	73.6	59.7	46.3	60	66	33.5	60.4	38.3/127.8
H_2 consump.(mmol)	0.006	0.005	0.004	0.003	0.005	0.005	0.007	0.006	0.006/0.012

The calcined photocatalysts have also been characterized by XPS; O 1s, Ti 2p, Pt 4f, Ga 2p, In 3d, Fe 2p and Ru 3d core levels were analyzed as shown in Figure 8.a, 8.b, 8.c, 8.d, 8.e, 8.f and 8.g.

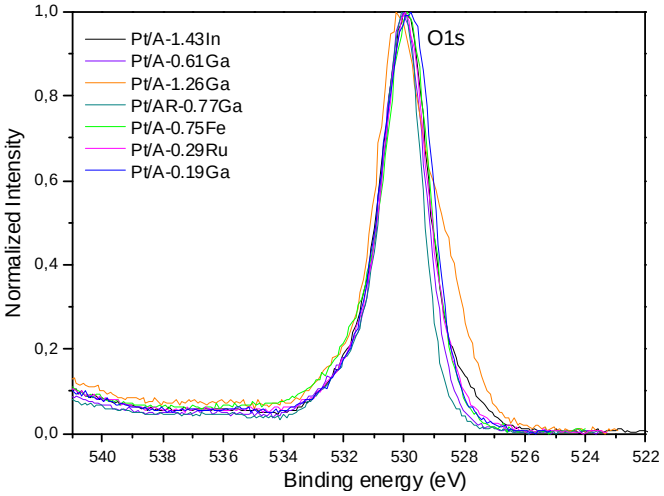

Figure 8.a. XPS spectra corresponding the O 1s core level of the photocatalysts

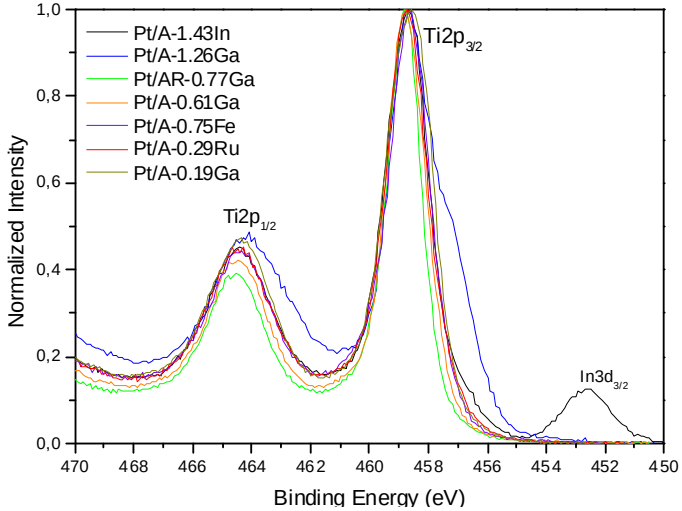

Figure 8.b. XPS spectra corresponding the Ti 2p core levels of the photocatalysts

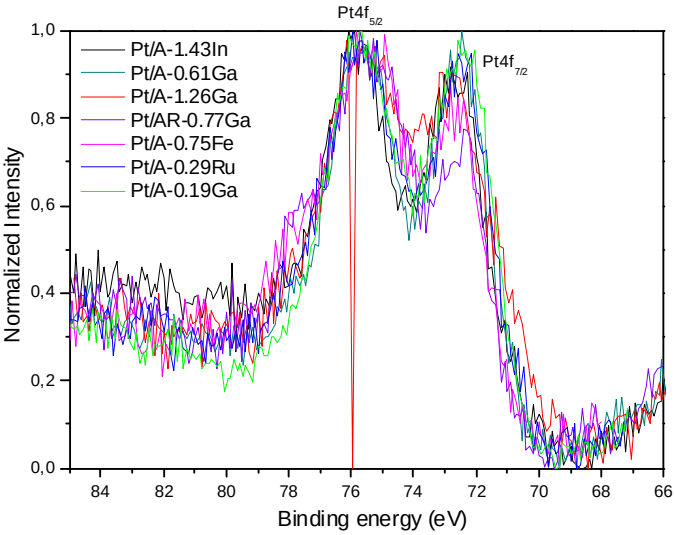

Figure 8.c. XPS spectra corresponding the Pt 4f core levels of the photocatalysts

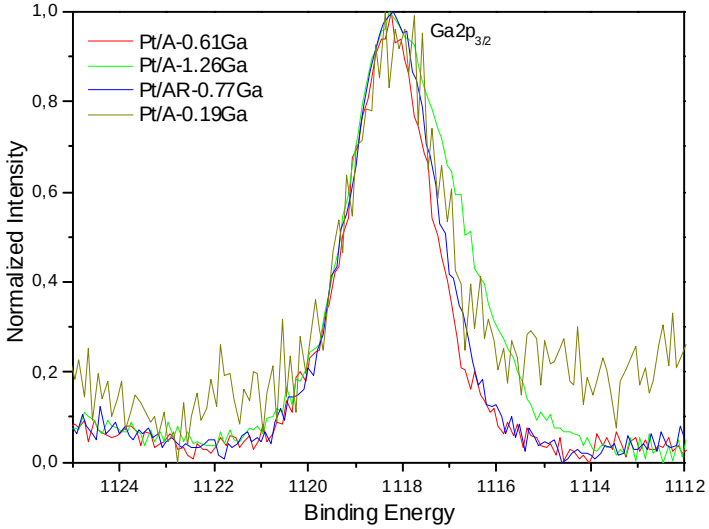

Figure 8.d. XPS spectra corresponding the Ga 2p core levels of the photocatalysts

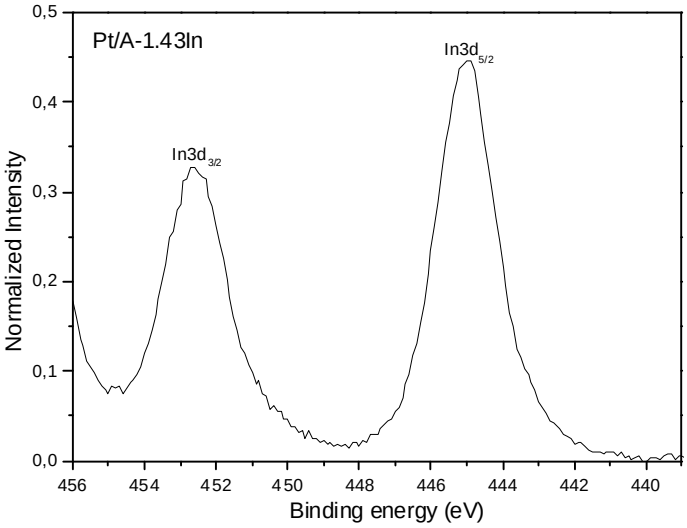

Figure 8.e. XPS spectra corresponding the In 3d core levels of Pt/A-1.43In

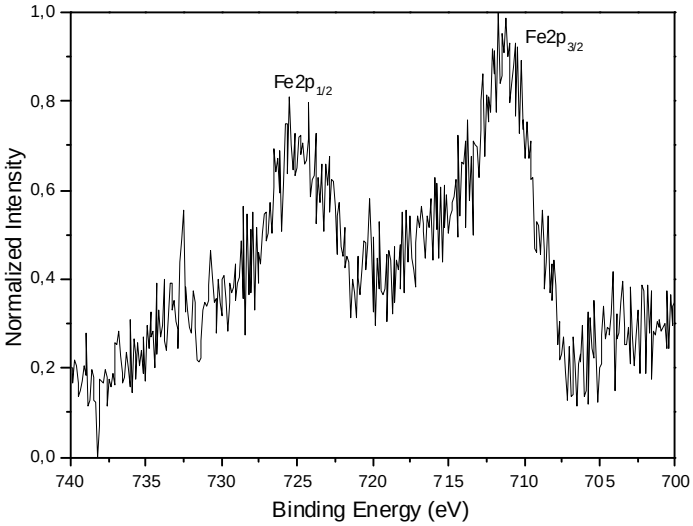

Figure 8.f. XPS spectra corresponding the Fe 2p core levels of Pt/A-0.75Fe

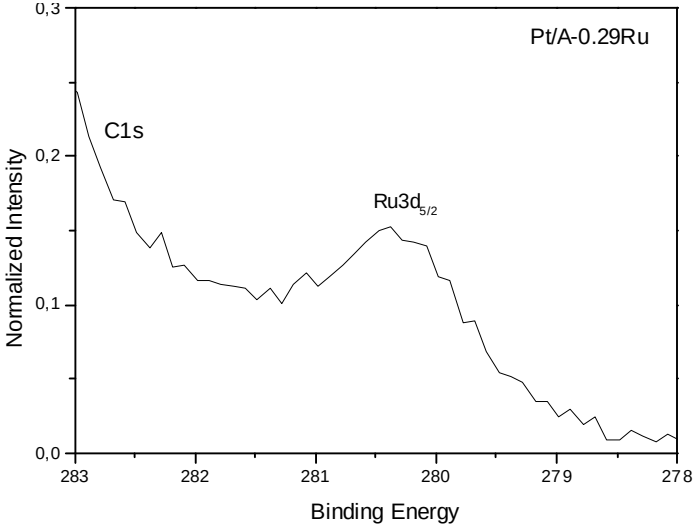

Figure 8.g. XPS spectra of the Ru 3d core level of Pt/A-0.29Ru

The BE for the core level O 1s of all the samples is 530±0.1 eV (Figure 8.a), which corresponds to previous BE values for this core level of oxide in TiO_2 [25]. Moreover, the O 1s peak is not symmetric with a slight shoulder at higher BE, and this could be due to a minor contribution of a different oxide which commonly can be superficial OH^-. The peak of this core level in Pt/A-1.26Ga is wider than in the other catalysts, this could be because it is the sample with the highest content of co-doped metal, and it has a different chemical environment.

Figure 8.b reveals the XPS spectra of the core levels of Ti $2p_{3/2}$ and Ti $2p_{1/2}$. The BE value of Ti $2p_{3/2}$ is 458.7±0.1 eV, corresponding to literature values of this core level for Ti(IV) in TiO_2 [25]. Both Ti $2p_{3/2}$ and Ti $2p_{1/2}$ core levels of the Pt/A-1.26Ga sample present a shoulder on the right side at lower BE, which is commonly associated to Ti(III). In this XPS spectra the In $3d_{3/2}$ can be found, which will be commented below.

Figure 8.c shows the XPS spectra of the core levels Pt $4f_{5/2}$ and Pt $4f_{7/2}$ of the photocatalysts. The peak of the Pt $4f_{7/2}$ in this spectra is wide with a maximum BE value at 72.65 eV. In the BE region of this core level, different Pt species can be found such as PtO_2, PtO and even Pt^0 [26]. The BE where the peaks of the core levels appear also depends on the chemical environment, so it cannot be confirmed which exact Pt species are present; probably a mixture of them.

Figure 8.d reveals the XPS spectra of the core level Ga $2p_{3/2}$ of the Ga containing photocatalysts. The BE of the peak of Ga $2p_{3/2}$ is 1118.19±0.2 eV, which is in concordance with the values of Ga_2O_3 1117-1118 eV [27].

Figure 8.e shows the XPS spectra of the core level In $3d_{5/2}$ of the Pt/A-1.43In sample. The BE value of the peak of In $3d_{5/2}$ in this spectra appears at 445 eV; this core level in In_2O_3 can be found at a BE of 444.2 eV, and in In_2O_3/TiO_2 at higher BE [8].

Figure 8.f shows the XPS spectra of Fe $2p_{1/2}$ and Fe $2p_{3/2}$ of the Pt/A-0.75Fe sample. The peak of the Fe $2p_{3/2}$ core level, in this case situated around BE= 711 eV, can indicate that the iron is present in form of Fe_2O_3 [27].

Figure 8.g shows the XPS spectra of the core level Ru $3d_{5/2}$ of the Pt/A-0.29Ru sample. In this case, it is difficult to assign the oxidation state of ruthenium due to its low intensity and its proximity to the C 1s core level. Previous works that have studied Ru/TiO_2 assign BE values of Ru $3d_{5/2}$ around 280.7 eV as possible presence of Ru as cations. Moreover, sources of XPS match similar BE to RuO_2, RuO_x and Ru^0 [28], so it cannot be exactly known which Ru species are present in the sample.

Table 3 lists the ratios $(Pt/Ti)_{ICP}$ and $(Pt/Ti)_{XPS}$, $(Pt/(M+Ti))_{XPS}$ and $(M/Ti)_{XPS}$

Table 3. ICP and XPS atomic ratios of the photocatalysts

SAMPLE	$(Pt/Ti)_{ICP}$	$(Pt/Ti)_{XPS}$	$(Pt/(Ti+M))_{XPS}$	$(M/Ti)_{XPS}$
Pt/A-1.43In	0.00193	0.0173	0.0163	0.1025
Pt/A-0.19Ga	0.00217	0.0183	0.0163	0.0163
Pt/A-0.61Ga	0.00201	0.0163	0.0152	0.0672
Pt/A-1.26Ga	0.00194	0.0142	0.0132	0.1377
Pt/AR-0.77Ga	0.00196	0.0132	0.0111	0.0764
Pt/A-0.75Fe	0.00208	0.0163	0.0162	0.0730
Pt/A-0.29Ru	0.00201	0.0183	0.0183	0.0050

Although all photocatalysts have a similar Pt content and ICP shows that the $(Pt/Ti)_{ICP}$ is similar between them, the $(Pt/Ti)_{XPS}$ is rather different. The behaviour that can be noted in all photocatalysts is that $(Pt/Ti)_{XPS}$ is considerably higher than $(Pt/Ti)_{ICP}$, which reveals that the segregation of platinum in TiO_2 on the surface is high.

In the gallium catalysts, the behaviour of Pt/AR-0.77Ga is slightly different from the others; although $(Pt/Ti)_{ICP}$ is similar to Pt/A-1.26Ga, $(Pt/Ti)_{XPS}$ is lower, which could mean that the platinum segregation is better in A than in AR when gallium is present.

Figure 8.h shows the relation between $(M/Ti)_{XPS}$ and the M loading per nm^2 of support of the photocatalysts. As can be observed, the segregation of metal is not always constant: it depends most of all on metal and also on its content. In the gallium samples, the relation between the ratios is linear. The surface segregation of indium is similar to the one of the gallium samples. It seems that ruthenium and iron have the worst surface segregation

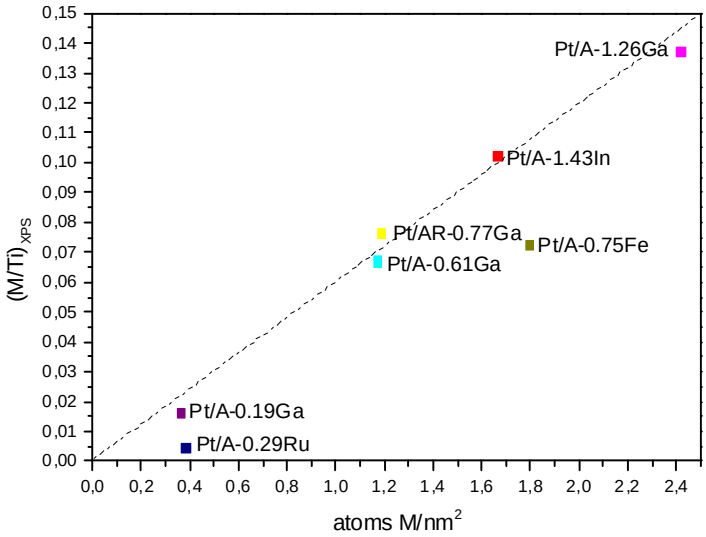

Figure 8.h $(M/Ti)_{XPS}$ vs. M atoms/nm² of support

7. CONCLUSIONS

-Pt/TiO_2-M (M=In, Ga, Fe, Ru) photocatalysts have successfully been prepared using two different supports, with the desired content of Pt and within the expected range of M loading per nm² of support.

-The crystalline phase of TiO_2 has not been affected by the metal deposition and the following thermal treatment in neither of the supports. As well as in A, in the Pt/A-M photocatalysts the anatase phase is clearly observed by XRD and Raman spectra and a very low content of rutile phase can be seen by XRD. In AR and in the Pt/AR-M samples, both anatase and rutile phases are clearly appreciable by XRD and Raman spectra and the ratio anatase:rutile of the support has not changed after its treatment. Moreover, the crystallite size of both supports has barely changed. This information leads to the conclusion that the structural characteristics of TiO_2 are not affected by the deposition of these metals in this wt% range.

-The N_2 adsorption/desorption isotherm of A and AR is type IV with an hysteresis loop type H1, which corresponds to mesoporous solids, and has not been affected by the metal deposition. The pore size distribution of A is in the range of 20-30 nm, and has not changed in the Pt/A-M photocatalysts. The pore size distribution of AR, which is wide, becomes highly narrow around 30 nm in the Pt/AR-M photocatalysts, having a similar pore size than the Pt/A-M photocatalysts. The surface area and the pore volume of the prepared photocatalysts have similar values to the supports. The achieved pore size distribution of the Pt/AR-M catalysts similar to the distribution of the Pt/A-M catalysts, together with the equal content of Pt and other similar properties, make the prepared photocatalysts worth to be compared in further studies of reaction.

-The Pt/A-M and Pt/AR-M catalysts have smaller band gap values than the supports, possibly due to the introduction of an intermediate state between the valence band and the conduction band of the support. The Eg decrease has been higher in the catalysts containing Fe and Ru than in the others.

-TPR has shown that the experimental H_2 consumption for the photocatalysts reduction has been higher than the maximum required to reduce the content of Pt in its maximum possible oxidation state, 4^+. This can indicate that also partial reduction of the co-doped metal oxide is taking place. The exception to this behaviour is the sample with less content of Ga (Pt/A-0.19Ga). The reduction peaks in the Pt/AR-M samples appear at lower temperatures than the Pt/A-M catalysts, which can indicate a better affinity of Pt with AR than with A, possibly due to the presence of rutile. Moreover, the reduction of the co-doped metals takes place at low temperatures because of the H_2 spillover effect by Pt.

-The XPS study has shown that the O 1s core level corresponds to TiO_2 oxide. Its asymmetry can indicate that superficial OH^- are also present. The Ti $2p_{3/2}$ core level indicates the presence of Ti(IV). Moreover, the shape of O 1s and Ti $2p_{3/2}$ in the sample Pt/A-1.26Ga (most M content) is wider than these core levels in the other samples. This could indicate a different chemical environment and the presence of Ti(III) species. The core level Pt $4f_{7/2}$ possibly indicates that platinum is present in a mixture of oxidation states 4^+ and 2^+. The core levels Ga $2p_{3/2}$, In $3d_{5/2}$, Fe $2p_{3/2}$ and Ru $3d_{5/2}$ indicate that the co-doped metals are probably in form of oxides.

-By XPS and ICP, the ratio Pt/Ti has been compared in the photocatalysts bulk and surface, and there is evidence of a high platinum segregation to the TiO_2 surface, which seems better in A than in AR. Moreover, the segregation of M has been studied: $(Ga/Ti)_{ICP}$ and $(Ga/Ti)_{XPS}$ follow

a linear relation. The behaviour of the In segregation is similar to Ga. Nevertheless, the surface segregation of Fe and Ru appears to be lower.

-Taking into account that high platinum segregation and low values of band gap are relevant characteristics for good photocatalytic activity of TiO_2, the photocatalysts prepared for this research work are highly relevant to be tested in reaction in further studies.

8. REFERENCES AND NOTES

1. Haiqiang Lu, Jianghong Zhao, Li Li, Liming Gong, Jianfeng Zheng, Lexi Zhang, Zhijian Wang, Jian Zhang and Zhenping Zhu. Energy Environ. Sci., 2011, 4, 3384.
2. Dennis Y. C. Leung, Xianliang Fu, Cuifang Wang,Meng Ni,Michael K. H. Leung, Xuxu Wang, and Xianzhi Fu. ChemSusChem 2010, 3, 681 – 694.
3. F. Albert Cotton, G. Wilkinson, C. A. Murillo, Manfred Bochmann, Advanced Inorganic Chemistry, 6th edition, John Wiley & Sons, 1999, pp. 695– 714.
4. D. E. Skinner, D. Philip Colombo, J. J. Cavaleri, R. M. Bowman . J. Phys. Chem. 1995, 99, 7853 –7856.
5. Rufino M. Navarro Yerga Dr., M. Consuelo Álvarez Galván Dr., F. del Valle, José A. Villoria de la Mano and José L. G. Fierro Prof. ChemSusChem 2009, 2, 471 –485
6. J. S. Jang, S. H. Choi, H. G. Kim, J. S. Lee. J. Phys. Chem. C 2008, 112, 17200– 17205
7. H.S. Mazloomi Tabaei, M. Kazemeini, M. Fattahi Scientia Iranica. 2012, 19(6),1626–1631
8. Junbo Zhong, Jianzhang Li, Jun Zeng, Xiyang He, Shengtiang Huang, Weidong Jiang, Minjiao Li. Appl. Phys A 2014,115, 1231–1238
9. R.A. van Santen, P.W.N.M. van Leeuwen, J.A. Moulijn, B.A. Averill (1999). *CATALYSIS: AN INTEGRATED APPROACH.* Elsevier. Amsterdam-Lausanne-New York-Oxford-Shannon-Singapore-Tokyo
10. http://particle.dk/methods-analytical-laboratory/surface-area-bet/surface-area-bet-theory June 2014
11. http://cma.tcd.ie/misc/Surface_area_and_porosity.pdf June 2014
12. K. S. W. Sing. Pure and Applied Chemistry 1985, 57, 4: 603–619
13. http://content.piacton.com/Uploads/Princeton/Documents/Library/UpdatedLibrary/Raman_Spectroscopy_Basics.pdf June 2014

14. http://www.micromeritics.com/Repository/Files/Autochem%20II%202920%20technique%20TPR.pdf June 2014
15. D. Briggs and M.P. Seah (Editors), *Practical Surface Analysis by Auger and X-Ray Photoelectron Spectroscopy*, Wiley, New York, 1983
16. http://www.eag.com/mc/inductively-coupled-plasma-spectroscopy.html June 2014
17. Dong Suk Kim, Seung-Yeop Kwak. Applied Catalysis A: 2007, 323, 110–118
18. H. Zhang, J.F. Banfield. J. Phys. Chem. 2000, B 104, 3481-3487
19. *Shimadzu* Application News, *No.A428*
20. Kairat Sabyrov , Vanessa Adamson and R. Lee Penn. CrystEngComm 2014,16,1488
21. Enjun Wang, Wensheng Yang and Yaan Cao. *J. Phys. Chem. C*, 2009, *113* (49), pp 20912–20917
22. F.D. Hardcastle. Journal of the Arkansas Academy of Science 2011 Vol. 65
23. Jean Rouquerol, Françoise Rouquerol, Philip Llewellyn, Guillaume Maurin, Kenneth S.W. Sing. *Adsorption by Powders and Porous Solids: Principles, Methodology and Applications*. Academic Press, 6/9/2013
24. Flávio FACCIN, Fabiana Flores GUEDES, Edilson Valmir BENVENUTTI, Celso Camilo MORO. Eclet. Quím. 2002 vol.27 (São Paulo)
25. M.C. Biesinger, L.W.M. Lau, A.R. Gerson, R.St.C. Smart, Appl. Surf. Sci. 2010, 257, 887
26. Tery L. Barr. J. Phys. Chem., 1978, 82, N° 16, 1801-1810
27. John F. Moulder, William F. Stickle, Peter E. Sobol and Kenneth D. Bomben. *Handbook of X-ray Photoelectron Spectroscopy*. Perkin-Elmer Corporation 1992
28. Lin, Xiahui ; Yang, Kai ; Si, Ruiru ; Chen, Xun ; Dai, Wenxin ; Fu, Xianzhi. Applied Catalysis B: Environmental 2014, 147:585-591

9. ACRONYMS

XRD: X-ray diffraction

BET: Brunauer-Emmet-Teller

DRS: UV–Vis diffuse reflectance spectroscopy

TPR: temperature-programmed reduction

XPS: X-ray photoelectron spectroscopy

ICP: Inductively coupled plasma spectrometry

Eg: band gap

VB: valence band

CB: conduction band

NHE: normal hydrogen electrode

EDTA: Ethylenediaminetetraacetic acid

RT: Room Temperature

BE: binding energy

M: metal

HPLC: High performance liquid chromatography

A: Sigma Aldrich TiO_2

AR: Degussa P25 TiO_2

JCPDS: Joint Committee Powder Diffraction Standards

APPENDICES

Figure 3.b. Raman spectra of A, Pt/A-Ru and Pt/A-Fe samples

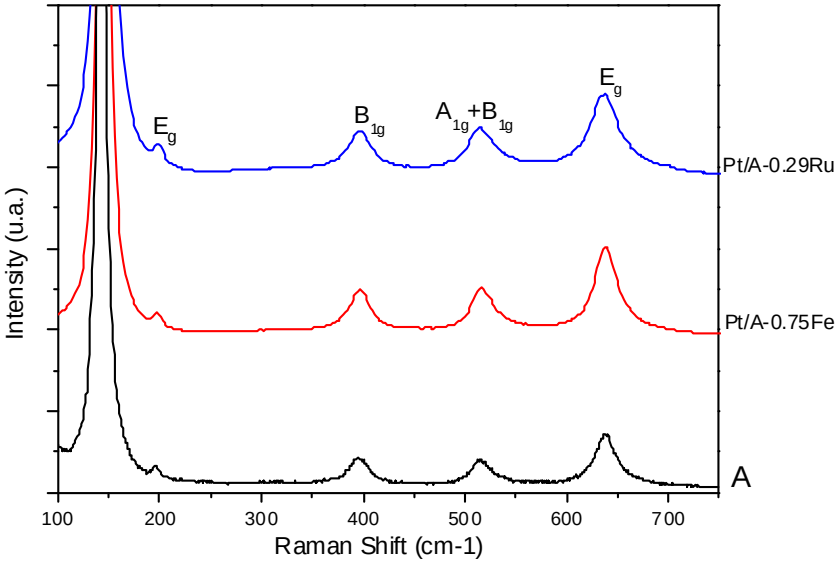

Figure 4.b. N_2 adsorption/desorption isotherm of A, Pt/A-Ru and Pt/A-Fe samples

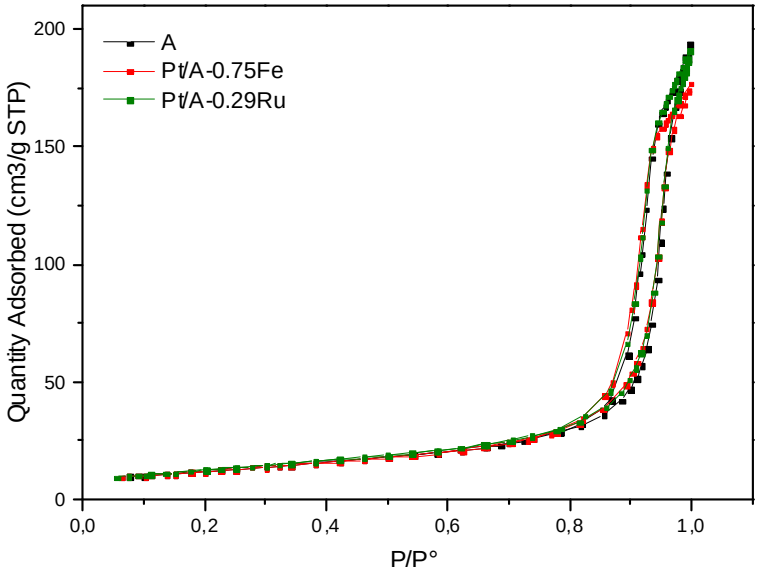

Figure 4.c. N_2 adsorption/desorption isotherm of AR, Pt/AR-In and Pt/AR-Ga samples

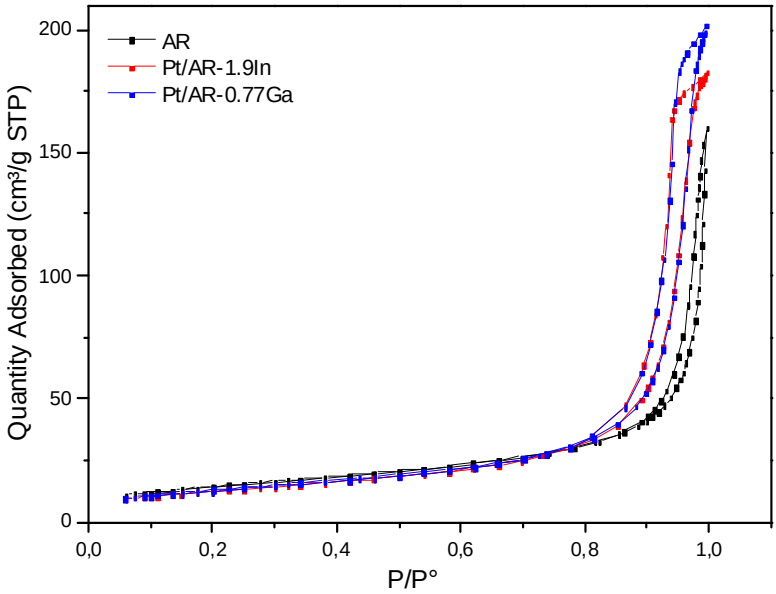

Figure 5.b. Pore size distribution of A, Pt/A-Ru and Pt/A-Fe samples

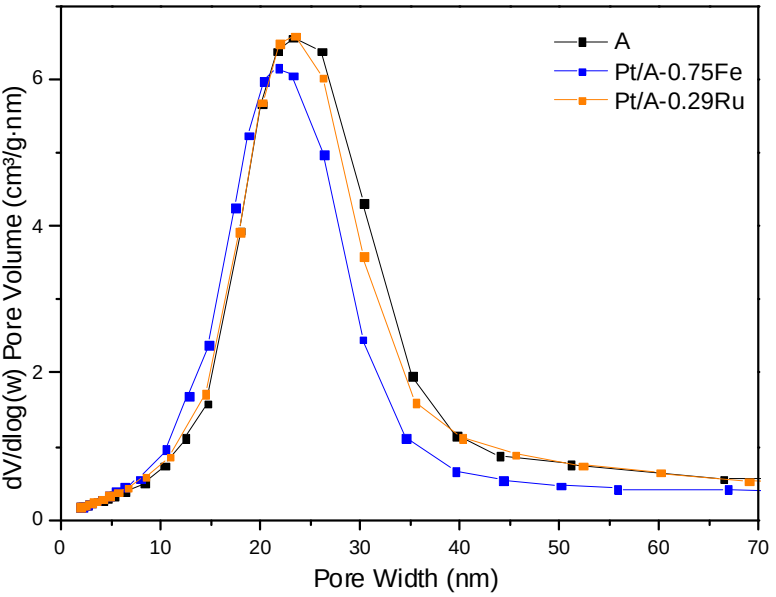

Figure 6.b. Tauc-Plot representation of A, Pt/A-0.75Fe and Pt/A-0.29Ru

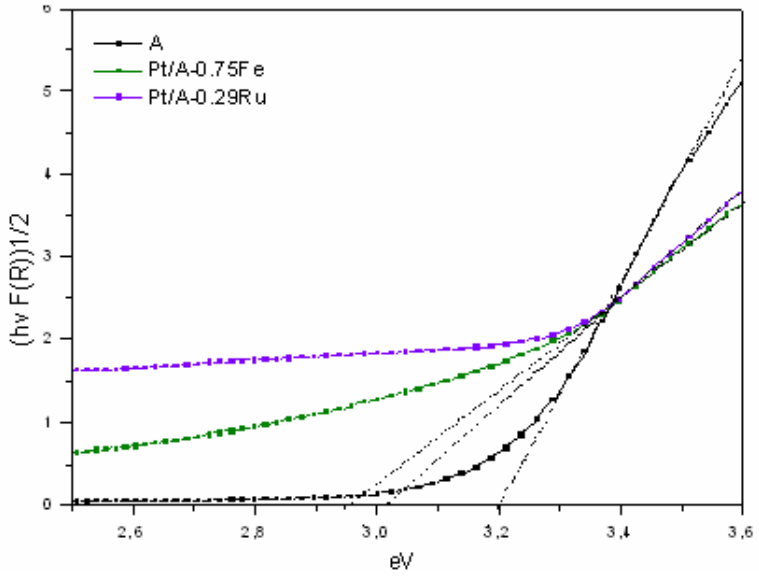

Figure 6.c. Tauc-Plot representation of AR, Pt/AR-1.9In and Pt/AR-0.77Ga